Supporting Information

A nine-coordinated dysprosium(III) compound with oxalate-bridged dysprosium(III) layer exhibiting two slow magnetic relaxation processes

Sheng Zhang,[a] Hongshan Ke,[a] Xiangyu Liu,[b] Qing Wei,[a] Gang Xie,[a] and Sanping Chen*[a]

[a] *Key Laboratory of Synthetic and Natural Functional Molecule Chemistry of Ministry of Education, College of Chemistry and Materials Science, Northwest University, Xi'an, Shaanxi 710069, PR China. E-mail: sanpingchen@126.com*

[b] *School of Chemistry and Chemical Engineering, Ningxia University, Yinchuan 750021, PR China*

Corresponding author

Dr Sanping Chen

E-mail: sanpingchen@126.com

1. Experimental

1.1. Materials and instrumentation

Commercially available reagents were used as received. The FT-IR spectra were recorded in the range of 400-4000 cm^{-1} using KBr pellets on an EQUINOX55 FT/IR spectrophotometer. Elemental analysis (C, H, N) was implemented on a Perkin−Elmer 2400 CHN elemental analyzer. The phase purity of the bulk or polycrystalline samples were confirmed by powder X-ray diffraction (PXRD) measurements executed on a Rigaku RU200 diffractometer at 60 kV, 300 mA, and Cu Kα radiation (λ = 1.5406 Å), with a scan speed of 5° min^{-1} and a step size of 0.02° in 2θ. Magnetic measurements were performed in the temperature range 1.9 K-300 K, using a Quantum Design MPMS-XL-7 SQUID magnetometer on polycrystalline samples. The diamagnetic corrections for the compounds were estimated using Pascal's constants.

1.2. Synthesis of compound $[Dy(C_2O_4)_{1.5}(H_2O)_3]_n \cdot 2nH_2O$ (1)

A mixed aqueous methanol (10mL, 1:1) of $Dy(ClO_4)_3 \cdot 6H_2O$ (0.0461 g, 0.10 mmol) and sodium oxalate (0.0402 g, 0.30 mmol) was heated in a Teflon-lined bomb (15 mL) at 90 °C for 3 days, slowly cooled to room temperature (5 °C h^{-1}). The purple crystals of **1** were isolated by filtrating, washing with aqueous methanol solution. (yield 57%, based on Dy). Anal. Calcd for $C_3H_8DyO_{10}$ (384.61): C, 9.36; H, 2.08 %. Found: C, 9.71; H, 2.25 %. Main IR (KBr, cm^{-1}): 3577 (s), 3432 (m), 1699 (m), 1633(s), 1559 (s), 1432 (s), 1422 (s), 1310 (m), 1255 (m), 1132 (m), 1022 (m), 987 (w), 787(m), 610 (w).

1.3. X-ray single-crystal diffraction analysis

The single crystal X-ray experiment was performed on a Rigaku SCX mini CCD diffractometer equipped with graphite-monochromatized Mo Kα radiation (λ = 0.71073 Å) using ω and φ scan mode. The data integration and reduction were processed with SAINT software. Absorption correction based on multiscan was performed using the SADABS program.[1] The structures were solved by the direct method using SHELXTL and refined by means of full-matrix least-squares procedures on F^2 with SHELXL-97 program.[2] All non hydrogen atoms were refined anisotropically. Other details of crystal data, data collection parameters, and refinement statistics are given in Table S1.The selected bond lengths and angles are listed in Table S2.

Table S1 Crystal data and structure refinement details for the compound **1**.

Compound	**1**
Empirical formula	C3H10DyO11
Formula weight	384.61
Temperature	296(2) K
Crystal system	Monoclinic
space group	$P2_1/c$
a (Å)	10.9675(14)
b (Å)	9.6145(12)
c (Å)	9.9881(12)
α (°)	90
β (°)	114.179(2)
γ (°)	90
V (Å^3)	960.8(2) A^3
Z	4
F(000)	728
Goodness-of-fit on F^2	1.011
Final R indices [I>2sigma(I)]	$R_1 = 0.0252$ $wR_2 = 0.0523$
R indices (all data)	$R_1 = 0.0295$ $wR_2 = 0.0545$
CCDC	1406485

Table S2. Selected bond lengths (Å) and angles (°) for **1**.

Compound **1**			
Dy(1)-O(4)	2.376(6)	O(5)-Dy(1)-O(7)	81.0(2)
Dy(1)-O(8)	2.379(7)	O(9)-Dy(1)-O(7)	137.0(3)
Dy(1)-O(5)	2.380(6)	O(2)-Dy(1)-O(7)	141.9(2)
Dy(1)-O(9)	2.387(7)	O(4)-Dy(1)-O(6)#1	71.6(2)
Dy(1)-O(2)	2.422(6)	O(8)-Dy(1)-O(6)#1	128.1(2)
Dy(1)-O(7)	2.442(7)	O(5)-Dy(1)-O(6)#1	66.6(2)
Dy(1)-O(6)#1	2.452(6)	O(9)-Dy(1)-O(6)#1	68.6(2)
Dy(1)-O(3)#2	2.460(6)	O(2)-Dy(1)-O(6)#1	136.9(2)
Dy(1)-O(1)#3	2.530(6)	O(7)-Dy(1)-O(6)#1	69.2(2)
O(1)-Dy(1)#3	2.530(6)	O(4)-Dy(1)-O(3)#2	66.8(2)
O(3)-Dy(1)#2	2.460(6)	O(8)-Dy(1)-O(3)#2	72.1(2)
O(6)-Dy(1)#1	2.452(6)	O(5)-Dy(1)-O(3)#2	141.0(2)
O(4)-Dy(1)-O(8)	137.2(2)	O(9)-Dy(1)-O(3)#2	129.0(2)
O(4)-Dy(1)-O(5)	138.2(2)	O(2)-Dy(1)-O(3)#2	69.7(2)
O(8)-Dy(1)-O(5)	73.3(2)	O(7)-Dy(1)-O(3)#2	72.3(2)
O(4)-Dy(1)-O(9)	75.9(2)	O(6)#1-Dy(1)-O(3)#2	125.4(2)
O(8)-Dy(1)-O(9)	143.5(3)	O(4)-Dy(1)-O(1)#3	140.4(2)
O(5)-Dy(1)-O(9)	89.9(2)	O(8)-Dy(1)-O(1)#3	69.9(3)
O(4)-Dy(1)-O(2)	82.3(2)	O(5)-Dy(1)-O(1)#3	66.3(2)

O(8)-Dy(1)-O(2)	94.4(3)	O(9)-Dy(1)-O(1)#3	73.6(3)
O(5)-Dy(1)-O(2)	130.7(2)	O(2)-Dy(1)-O(1)#3	64.7(2)
O(9)-Dy(1)-O(2)	72.1(2)	O(7)-Dy(1)-O(1)#3	136.1(2)
O(4)-Dy(1)-O(7)	83.4(3)	O(6)#1-Dy(1)-O(1)#3	118.2(2)
O(8)-Dy(1)-O(7)	73.3(3)	O(3)#2-Dy(1)-O(1)#3	116.4(2)

Symmetry transformations used to generate equivalent atoms:

#1 -x+1,-y+1,-z+1 #2 -x,-y+1,-z #3 -x,-y+1,-z+1

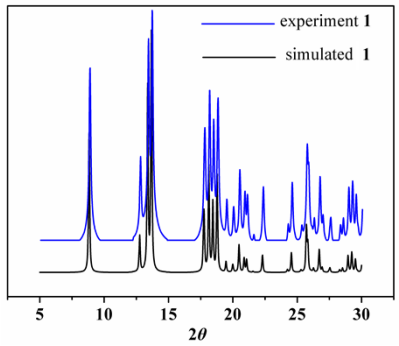

Figure S1. XRPD curve of **1.**

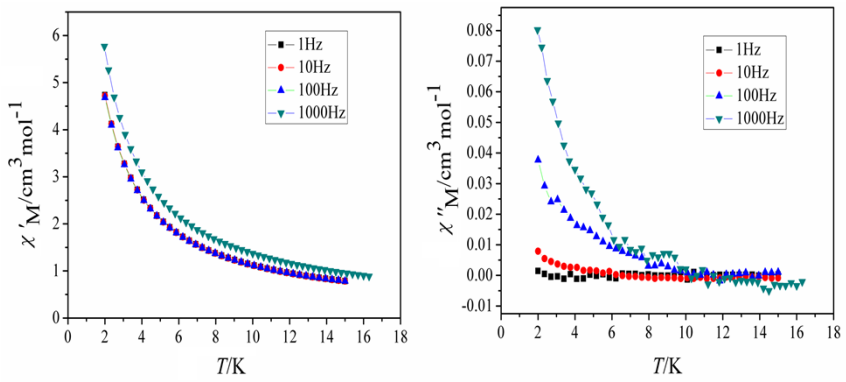

Figure S2. Temperature dependences of χ'_M (left) and χ''_M (right) of **1** measured range from 1Hz to 1000 Hz in an 0 Oe external dc field.

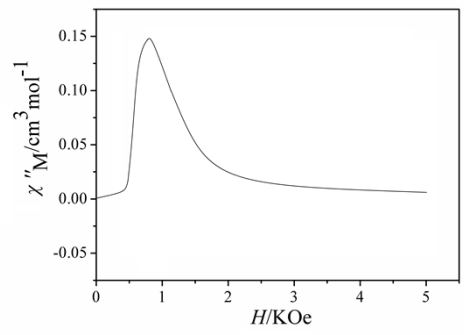

Figure S3. Dependence of the out-of-phase signal of **1** on applied dc field strength at 1.9 K, 1000 Hz. χ'' signal with a significant sharp peak around 700 Oe dc field indicates field-enhanced slow magnetic relaxation operating in **1**.

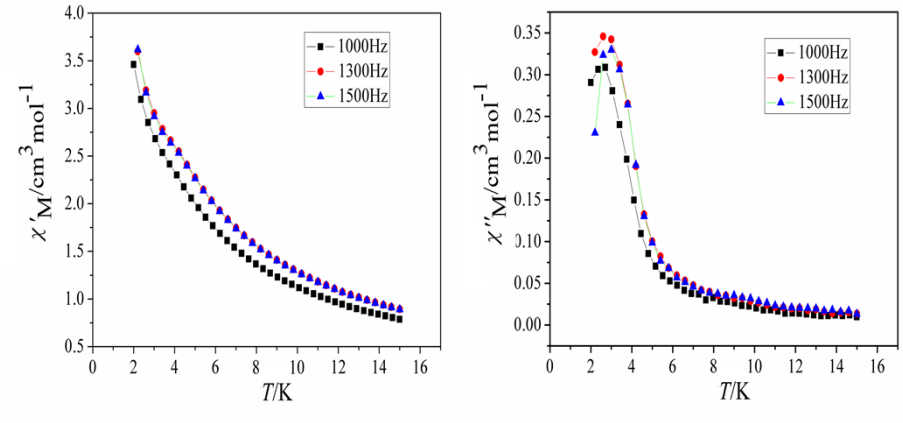

Figure S4. Temperature dependences of χ'_M (left) and χ''_M (right) component of **1** measured under an applied magnetic field of 700 Oe. As compared with the zero dc field (Figure S2), the intensity of out-of-phase susceptibility under the applied external dc field is dramatically enhanced.

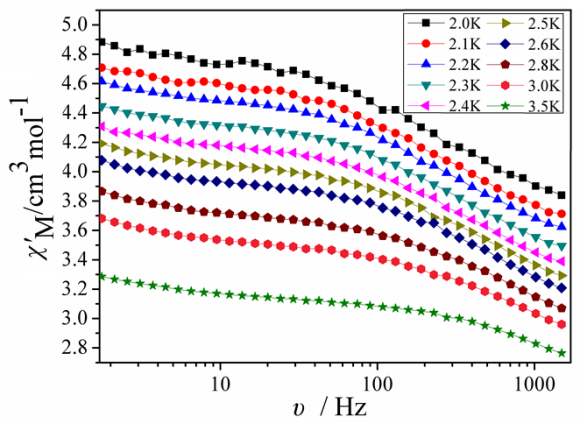

Figure S5. Frequency dependence of the in-of-phase χ'_M components of the alternating-current (ac) susceptibility for compound **1**, measured under an applied magnetic field of 700 Oe in the temperature range of 2.0–3.5 K.

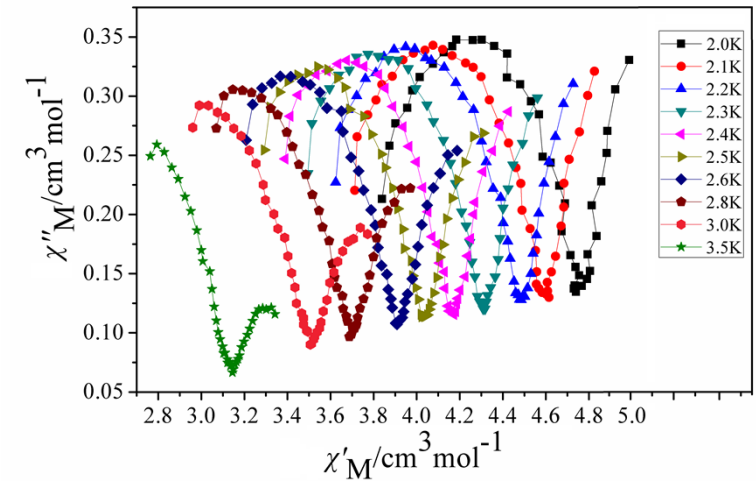

Figure S6. Cole–Cole plot for **1** under an applied magnetic field of 700 Oe at the indicated temperatures.

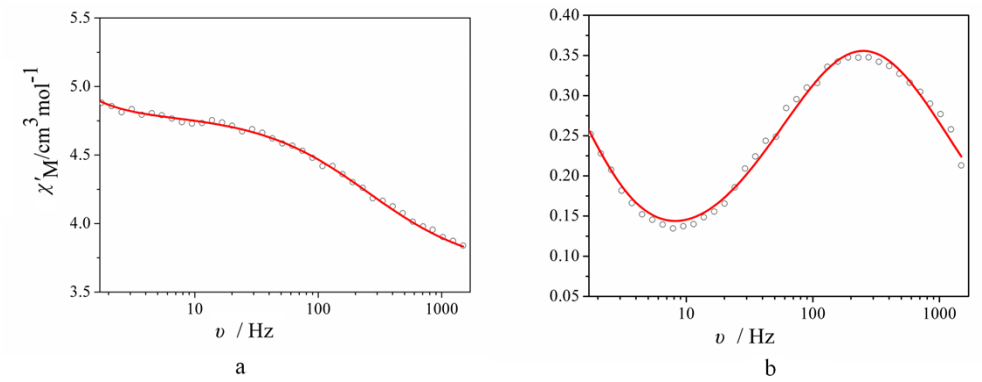

Figure S7. Frequency dependence of the in-of-phase (χ', right) and out-of-phase (χ'', left) ac susceptibility of **1** at 2.0 K. The full range plots can be fitted well by the following parameters: $\alpha_1 = 0.306$; $\alpha_2 = 0.012$; $\tau_1 = 6.26\times10^{-4}$ s; $\tau_2 = 0.220$ s; $\chi_{S,tot} = 3.641$ cm^{3}mol^{-1}; $\Delta\chi_1 = 1.167$ cm^{3}mol^{-1} ; $\Delta\chi_2 = 0.629$ cm^{3}mol^{-1}. The red lines are the fits of the full range plots.

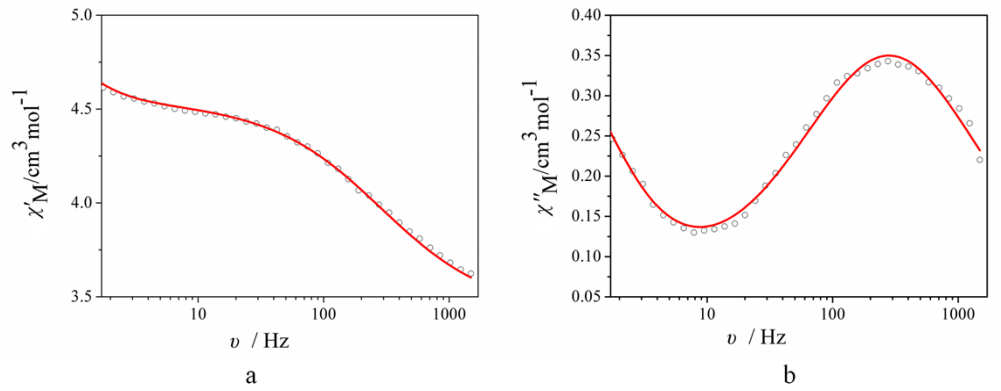

Figure S8. Frequency dependence of the in-of-phase (χ', right) and out-of-phase (χ'', left) ac susceptibility of **1** at 2.1 K. The full range plots can be fitted well by the following parameters: $\alpha_1 = 0.305$; $\alpha_2 = 0.015$; $\tau_1 = 5.57\times10^{-4}$ s; $\tau_2 = 0.216$ s; $\chi_{S,tot} = 3.400$ cm^{3}mol^{-1}; $\Delta\chi_1 = 1.146$ cm^{3}mol^{-1} ; $\Delta\chi_2 = 0.626$ cm^{3}mol^{-1}. The red lines are the fits of the full range plots.

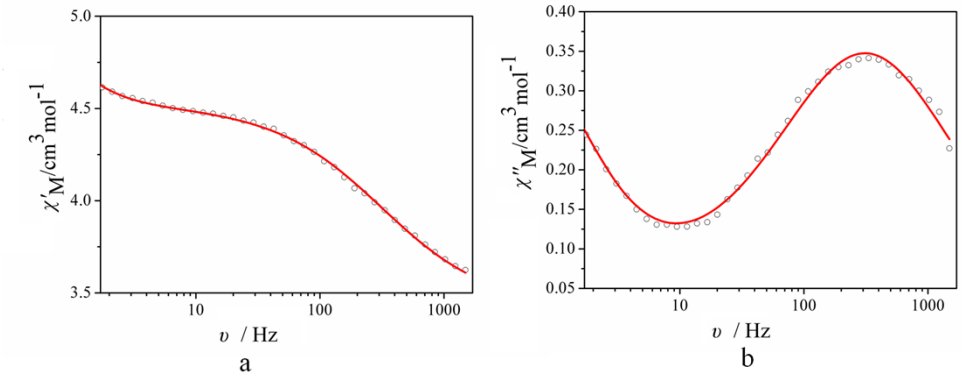

Figure S9. Frequency dependence of the in-of-phase (χ', right) and out-of-phase (χ'', left) ac susceptibility of **1** at 2.2 K. The full range plots can be fitted well by the following parameters: $\alpha_1 = 0.299$; $\alpha_2 = 0.035$; $\tau_1 = 5.05\times10^{-4}$ s; $\tau_2 = 0.212$ s; $\chi_{S,tot} = 3.399$ cm^{3}mol^{-1}; $\Delta\chi_1 = 1.126$ cm^{3}mol^{-1} ; $\Delta\chi_2 = 0.623$ cm^{3}mol^{-1}. The red lines are the fits of the full range plots.

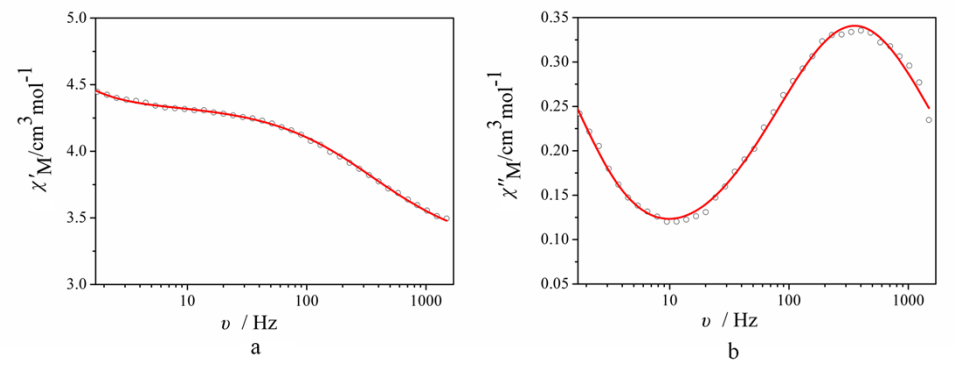

Figure S10. Frequency dependence of the in-of-phase (χ', right) and out-of-phase (χ'', left) ac susceptibility of **1** at 2.3 K. The full range plots can be fitted well by the following parameters: $\alpha_1 = 0.300$; $\alpha_2 = 0.025$; $\tau_1 = 4.43\times10^{-4}$ s; $\tau_2 = 0.208$ s; $\chi_{S,tot} = 3.250$ cm^{3}mol^{-1}; $\Delta\chi_1 = 1.107$ cm^{3}mol^{-1} ; $\Delta\chi_2 = 0.608$ cm^{3}mol^{-1}. The red lines are the fits of the full range plots.

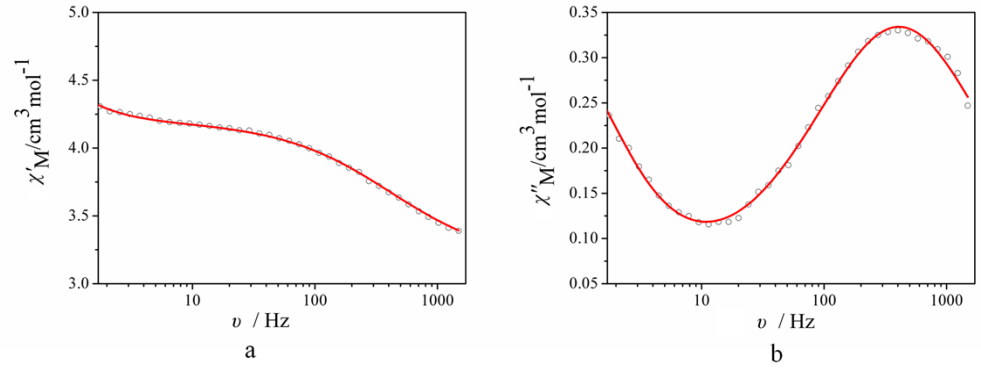

Figure S11. Frequency dependence of the in-of-phase (χ', right) and out-of-phase (χ'', left) ac susceptibility of **1** at 2.4 K. The full range plots can be fitted well by the following parameters: $\alpha_1 = 0.297$; $\alpha_2 = 0.055$; $\tau_1 = 3.84\times10^{-4}$ s; $\tau_2 = 0.204$ s; $\chi_{S,tot} = 3.145$ cm^{3}mol^{-1}; $\Delta\chi_1 = 1.097$ cm^{3}mol^{-1} ; $\Delta\chi_2 = 0.608$ cm^{3}mol^{-1}. The red lines are the fits of the full range plots.

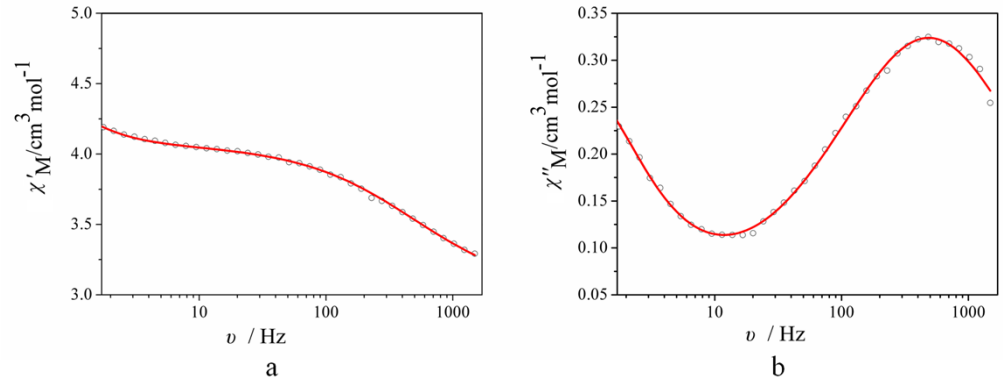

Figure S12. Frequency dependence of the in-of-phase (χ', right) and out-of-phase (χ'', left) ac susceptibility of **1** at 2.5 K. The full range plots can be fitted well by the following parameters: $\alpha_1 = 0.311$; $\alpha_2 = 0.056$; $\tau_1 = 3.23\times10^{-4}$ s; $\tau_2 = 0.184$ s; $\chi_{S,tot} = 3.001$ cm^{3}mol^{-1}; $\Delta\chi_1 = 1.073$ cm^{3}mol^{-1} ; $\Delta\chi_2 = 0.563$ cm^{3}mol^{-1}. The red lines are the fits of the full range plots.

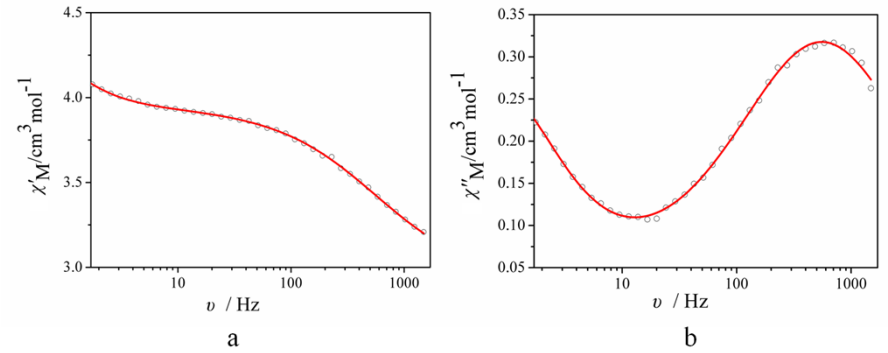

Figure S13. Frequency dependence of the in-of-phase (χ', right) and out-of-phase (χ'', left) ac susceptibility of **1** at 2.6 K. The full range plots can be fitted well by the following parameters: $\alpha_1 = 0.309$; $\alpha_2 = 0.084$; $\tau_1 = 2.84\times10^{-4}$ s; $\tau_2 = 0.179$ s; $\chi_{S,tot} = 2.900$ cm^{3}mol^{-1}; $\Delta\chi_1 = 1.048$ cm^{3}mol^{-1} ; $\Delta\chi_2 = 0.555$ cm^{3}mol^{-1}. The red lines are the fits of the full range plots.

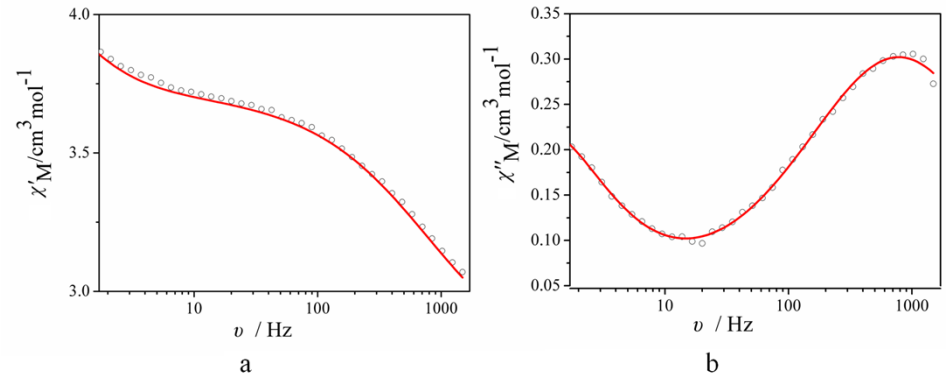

Figure S14. Frequency dependence of the in-of-phase (χ', right) and out-of-phase (χ'', left) ac susceptibility of **1** at 2.8 K. The full range plots can be fitted well by the following parameters: $\alpha_1 = 0.334$; $\alpha_2 = 0.115$; $\tau_1 = 2.01\times10^{-4}$ s; $\tau_2 = 0.165$ s; $\chi_{S,tot} = 2.670$ cm^{3}mol^{-1}; $\Delta\chi_1 = 1.043$ cm^{3}mol^{-1} ; $\Delta\chi_2 = 0.508$ cm^{3}mol^{-1}. The red lines are the fits of the full range plots.

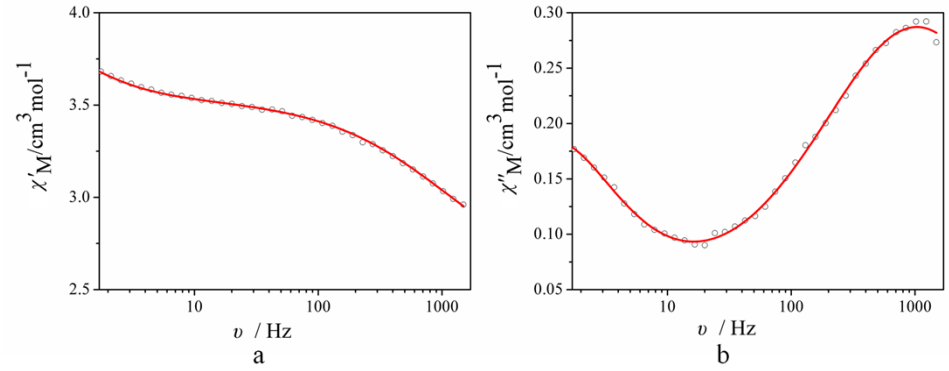

Figure S15. Frequency dependence of the in-of-phase (χ', right) and out-of-phase (χ'', left) ac susceptibility of **1** at 3.0 K. The full range plots can be fitted well by the following parameters: $\alpha_1 = 0.347$; $\alpha_2 = 0.138$; $\tau_1 = 1.52\times10^{-4}$ s; $\tau_2 = 0.144$ s; $\chi_{S,tot} = 2.520$ cm^{3}mol^{-1}; $\Delta\chi_1 = 1.016$ cm^{3}mol^{-1} ; $\Delta\chi_2 = 0.437$ cm^{3}mol^{-1}. The red lines are the fits of the full range plots.

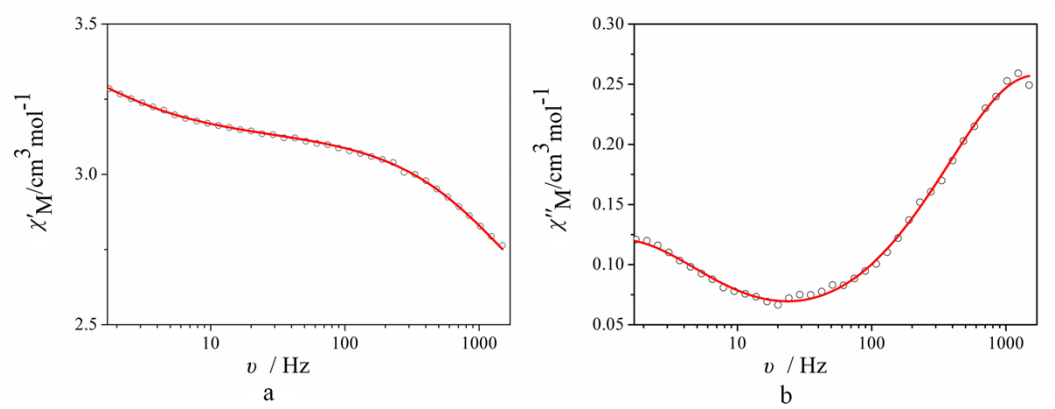

Figure S16. Frequency dependence of the in-of-phase (χ', right) and out-of-phase (χ'', left) ac susceptibility of **1** at 3.5 K. The full range plots can be fitted well by the following parameters: $\alpha_1 = 0.284$; $\alpha_2 = 0.280$; $\tau_1 = 9.65\times10^{-5}$ s; $\tau_2 = 0.126$ s; $\chi_{S,tot} = 2.324$ cm^{3}mol^{-1}; $\Delta\chi_1 = 0.810$ cm^{3}mol^{-1} ; $\Delta\chi_2 = 0.367$ cm^{3}mol^{-1}. The red lines are the fits of the full range plots.

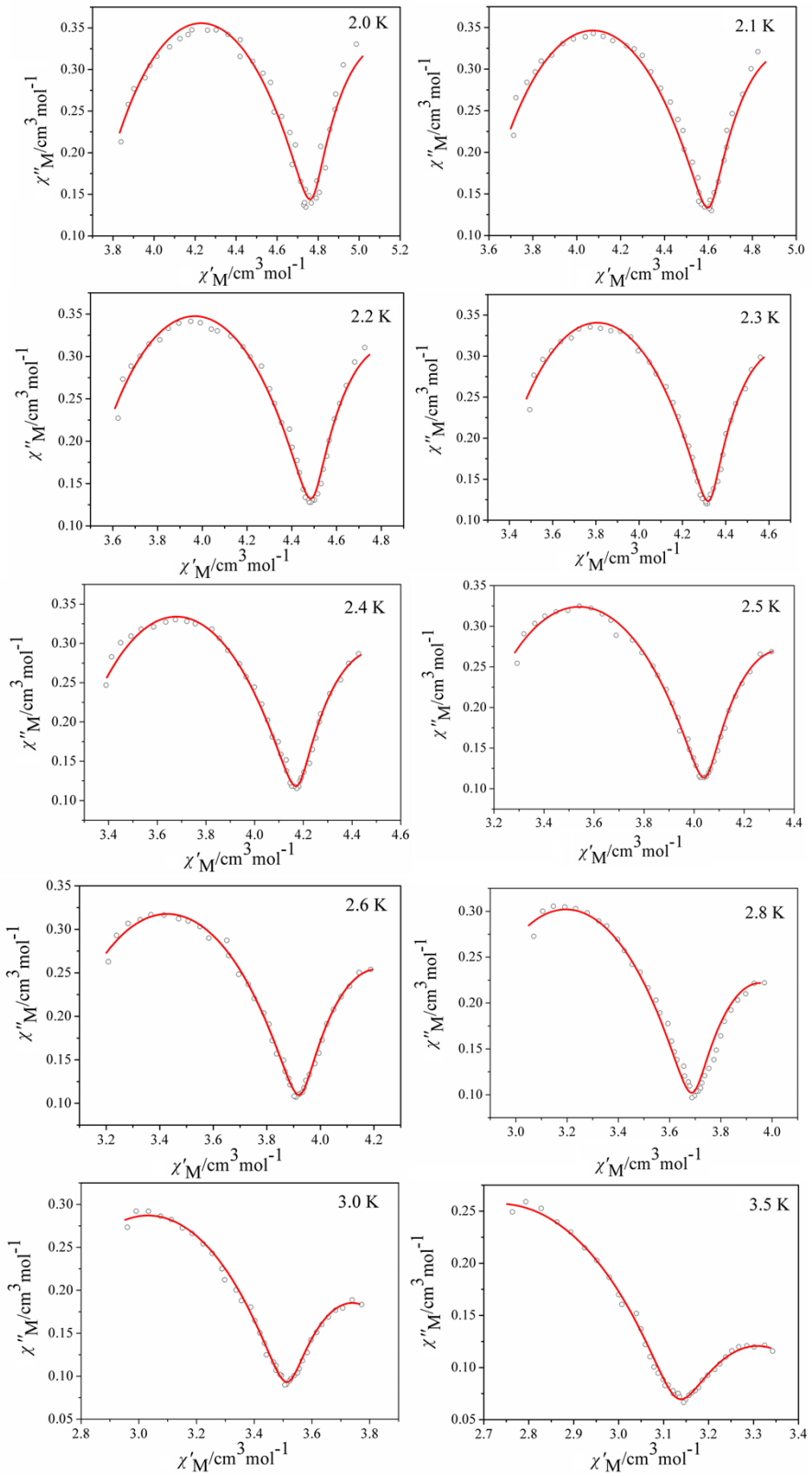

Figure S17. Simulations of dynamical susceptibility $\chi(\omega)$ ranging from 2.0 to 3.5 K in a Cole-Cole diagram. Red lines were performed using the sum of two modified Debye functions with the fitting parameters in Table S3.

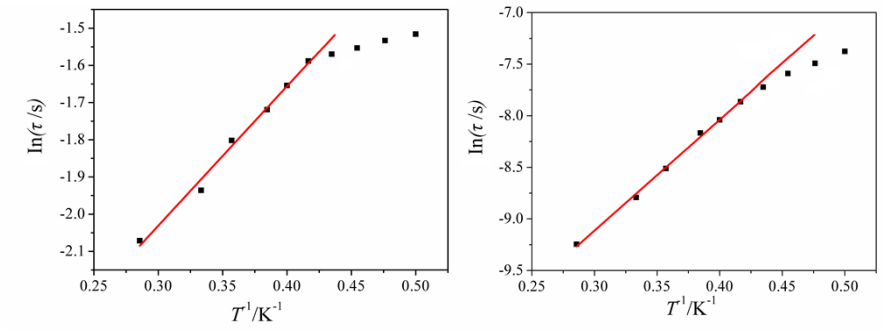

Figure S18. Relaxation time of the magnetization for **1** extracted from the frequency-dependent data between 2.0 and 3.5 K, by fitting the χ''_M vs. frequency curves (a): Fast relaxation phase. (b): Slow relaxation phase. The red lines are the fits of the thermally activated region.

The magnetic susceptibility data were described by the sum of two modified Debye functions:[3]

$$\chi''(\omega) = \Delta\chi_1 \frac{(\omega\tau_1)^{1-\alpha_1}\cos(\pi\alpha_1/2)}{1+2(\omega\tau_1)^{1-\alpha_1}\sin(\pi\alpha_1/2)+(\omega\tau_1)^{(2-2\alpha_1)}} + \Delta\chi_2 \frac{(\omega\tau_2)^{1-\alpha_2}\cos(\pi\alpha_2/2)}{1+2(\omega\tau_2)^{1-\alpha_2}\sin(\pi\alpha_2/2)+(\omega\tau_2)^{(2-2\alpha_2)}}$$

$\Delta\chi_1, \tau_1, \alpha_1, \Delta\chi_2, \tau_2, \alpha_2$

$$\chi'(\omega) = \chi_{S,tot} + \Delta\chi_1 \frac{1+(\omega\tau_1)^{1-\alpha_1}\sin(\pi\alpha_1/2)}{1+2(\omega\tau_1)^{1-\alpha_1}\sin(\pi\alpha_1/2)+(\omega\tau_1)^{(2-2\alpha_1)}} + \Delta\chi_2 \frac{1+(\omega\tau_2)^{1-\alpha_2}\sin(\pi\alpha_2/2)}{1+2(\omega\tau_2)^{1-\alpha_2}\sin(\pi\alpha_2/2)+(\omega\tau_2)^{(2-2\alpha_2)}}$$

$\chi_{S,tot}, \Delta\chi_1, \tau_1, \alpha_1, \Delta\chi_2, \tau_2, \alpha_2$

Table S3. Relaxation fitting parameters from Least-Squares Fitting of $\chi(\omega)$ data.

T(K)	$\chi_{S,tot}$ (cm^3mol^{-1})	$\Delta\chi_1$ (cm^3mol^{-1})	$\Delta\chi_2$ (cm^3mol^{-1})	α_1	α_2	τ_1(s)	τ_2(s)
2.0	3.641	1.167	0.629	0.306	0.012	6.26×10^{-4}	0.220
2.1	3.400	1.146	0.626	0.305	0.015	5.57×10^{-4}	0.216
2.2	3.399	1.126	0.623	0.299	0.035	5.05×10^{-4}	0.212
2.3	3.250	1.107	0.608	0.300	0.025	4.43×10^{-4}	0.208
2.4	3.145	1.079	0.608	0.297	0.055	3.84×10^{-4}	0.204
2.5	3.001	1.073	0.563	0.311	0.056	3.23×10^{-4}	0.184
2.6	2.900	1.048	0.555	0.309	0.084	2.84×10^{-4}	0.179
2.8	2.670	1.043	0.508	0.334	0.115	2.01×10^{-4}	0.165
3.0	2.520	1.016	0.437	0.347	0.138	1.52×10^{-4}	0.144
3.5	2.324	0.810	0.367	0.284	0.280	9.65×10^{-5}	0.126

Table S4. The reported relaxation mechanism about two or multiple relaxation processes.

Compound	τ_1(s), Δ_1(K)	τ_2(s), Δ_2(K)	Relaxation mechanism	Ref.
[(COT)Er(Cp*)], 0D	3.13×10^{-9}s, 197K	8.17×10^{-11}s, 323K	The complex displays two relaxation peaks attributed to the presence of two different conformers.	J. Am. Chem. Soc., 2011, **133**, 4730-4733.

$[Dy(H_2L)(NO_3)_3]\cdot 2CH_3OH$, 0D	2.4×10^{-5}s, 17.1K	1.3×10^{-7}s, 17.1K	The existence of two peaks was justified by the presence of applied field (or applied field on a diluted sample).	*Chem. Commun.*, 2012, **48**, 7916–7918.
$[Dy(COT)_2Li(THF)(DME)]$, 0D	Field-Induced Multiple Relaxation		The observed relaxation pathways strongly depend on the applied static dc fields.	*J. Am. Chem. Soc.*, 2011, **133**, 19286–19289.
$U(H_2BPz_2)_3$, 0D	Dilution-Induced Slow Magnetic Relaxation		These combined results highlight the impact of intermolecular interactions in mononuclear single-molecule magnets possessing a highly anisotropic metal center.	*Inorg. Chem.*, 2011, **50**, 8484–8489.
$[Dy^{III}Co^{III}_2(hmb)_2\text{-}(CH_3O)_2(OAc)_3]\cdot 2CH_3CN\cdot CH_3OH\cdot H_2O$, 0D	Field-Induced Multiple Relaxation		The field-tunable multiple thermally activated relaxation processes are of molecular and dipolar-dipolar coupling origin.	*Inorg. Chem.*, 2014, **53**, 12658−12663.
$[\{Dy^{III}(hfac)_3NitPhIm_2\}Dy(hfac)_3]$, 1D chain	17.5×10^{-6}s, 17.1K	8.8×10^{-8}s, 82.7K	The slow process was based on the 1D chain and disappeared in the diluted sample while the fast process was based on the "Rad-Tb···Rad" unit which was enhanced by removing the dipole-dipole interactions in diluted samples.	*Chem. Commun.*, 2010, **46**, 2566-2568.
$[Ln(hfac)_3(NITPhCOOMe)]$, 1D chain	0.059(3) s	2.0×10^{-8}s, 36K	The slow process was based on the 1D chain and disappeared in the diluted sample while the fast process was based on the "Rad-Tb···Rad" unit which was enhanced by removing the dipole-dipole interactions in diluted samples.	*Chem. Commun.*, 2015, **51**, 10933-10936.

H_2L = N,N',N''-trimethyl-N,N00-bis(2-hydroxy-3-methoxy-5-methylbenzyl) diethylene triamine; HPz = pyrazole; R = H, Ph; H_2hmb = 2-hydroxy-3-methoxybenzylidene benzohydrazide; NitPhIm = 2-[4-(1-imidazole)- phenyl]nitronyl nitroxide radical; hfac = hexafluoroacetyl acetonate; NITPhCOOMe = 2-(4-(methoxycarbonyl)phenyl)-4,4,5,5-tetramethylimidazolin-1-oxyl-3-oxide; Cp* = pentamethylcyclopentadienide; COT = cyclooctatetraenide.

References

1 Sheldrick, G. M. SADABS, Program for Empirical Absorption Correction; University of Göttingen, Göttingen, Germany, 1996.

2 Sheldrick, G. M.SHELXTL; Bruker Analytical X-ray Instruments, Inc.: Madison, WI, 1998.

3 G. Cuccinota, M. Perfetti, J. Luzon, M. Etienne, P. E. Car, A. Caneschi, G. Calvez, K. Bernot and R. Sessoli, *Angew. Chem. Int. Ed.*, 2012, **51**, 1606-1610.